Chemical Science

ROYAL SOCIETY OF CHEMISTRY

EDGE ARTICLE

View Article Online
View Journal | View Issue

Cite this: *Chem. Sci.*, 2025, **16**, 2609

All publication charges for this article have been paid for by the Royal Society of Chemistry

Received 30th November 2024
Accepted 5th January 2025

DOI: 10.1039/d4sc08125k

rsc.li/chemical-science

Electrolyte design weakens lithium-ion solvation for a fast-charging and long-cycling Si anode†

Min Li, [ab] Shuai Li,[a] Dong Yan,[a] Yuhao Ma,[a] Xiaobin Niu [a] and Liping Wang *[a]

Silicon (Si) is considered a promising anode material for next-generation lithium-ion batteries due to its high theoretical specific capacity and earth-abundancy. However, challenges such as significant volume expansion, unstable solid electrolyte interphase (SEI) formation in incompatible electrolytes, and slow lithium-ion transport lead to its poor cycling and rate performance. In this work, it is demonstrated that superior cyclability and rate capability of Si anodes can be achieved using ethyl fluoroacetate (EFA) and fluoroethylene carbonate (FEC) solvents with low binding energy with Li^+ but with sufficiently high relative dielectric constants. By weakening the interaction between Li^+ and the solvent, the energy barrier for the Li^+ desolvation process is lowered, while ensuring the conductivity and diffusion of Li^+. As a result, the silicon–carbon anode with the optimized electrolyte exhibits excellent cycling and rate performance, and can work reversibly with a high capacity of 1709.1 mAh g^{-1} that proceeds for over 250 cycles and retains 85.2% of its capacity at 0.2C. Furthermore, the Si/C||$LiFePO_4$ (LFP) full cell shows an extended service life of more than 500 cycles. This work offers valuable insights into the design of weakly solvating electrolytes for high-performance Si-based batteries.

1 Introduction

With the development of electric vehicles and large-scale energy storage systems, existing commercial lithium-ion batteries (LIBs) are increasingly unable to meet the market's demand. For this reason, researchers have explored various novel material systems to increase the energy density of batteries, such as alloy-based anodes,[1,2] Li metal anodes,[3,4] sulfide-based cathodes,[5–7] and Li-rich manganese-based cathodes.[8,9] Among these, silicon (Si) is regarded as one of the best alternatives to the commercial graphite anode due to its outstanding advantage of high theoretical capacity (4200 mAh g^{-1}) and appropriate operating voltage (~0.4 V, *vs.* Li/Li^+).[10] However, the volume expansion of the silicon is up to 300% upon lithiation, and the repeated insertion and extraction of Li^+ induce mechanical stress and deformation on the surface, leading to the pulverization of particles.[11] The volume deformation disrupts electrical contact between adjacent silicon particles or between the particles and the current collector, with active materials potentially detaching entirely from the collector.[10,12] Additionally, the solid electrolyte interphase (SEI) on the silicon surface repeatedly ruptures and regenerates as a result of the volumetric deformation of silicon, consuming substantial amounts of electrolyte and active lithium.[13] Over time, the increasing thickness of the SEI further degrades the Coulombic efficiency and ionic conductivity of LIBs.[14]

The electrolyte is a crucial component in Si-based LIBs, with its formulations essential for enhancing battery kinetics. It not only determines the mobility and desolvation of ions but also serves as the precursor for the SEI.[15] Li^+ migration within a battery involves four primary steps: the migration of solvated Li^+ in the native electrolyte, the desolvation process of solvated Li^+, the migration of Li^+ across the SEI, and the diffusion of Li^+ in the electrode materials.[16] The rate of these steps can be affected by various factors, such as the thickness and porosity of the electrode, the particle size of active materials, and the operating temperature.[17] Among these processes, the desolvation process of Li^+ is considered the primary energy-consuming and rate-limiting step, particularly in fast-charging and low-temperature applications.[18] In conventional electrolytes, the highly solvated ethylene carbonate (EC) molecules are firmly bound to Li^+ with high viscosity and a large molecular structure, hindering the detachment of Li^+ from its solvated sheath at the anode interface of the battery, resulting in a highly polarized interface which leads to a decrease in battery capacity or the formation of lithium dendrites.[19] Additionally, the conventional EC-based electrolyte is prone to continuous reaction and decomposition on the surface of silicon anodes, and repeated cracking/crushing occurs at the interface, resulting in electrolyte drying and sudden capacity degradation.[20] Therefore, the Si anode is subjected to excessive SEI growth, further increasing the barrier to transport Li^+ at the electrode/electrolyte interface.[21]

[a]*School of Materials and Energy, University of Electronic Science and Technology of China, Chengdu 611731, China. E-mail: lipingwang@uestc.edu.cn*

[b]*Tianmu Lake Institute of Advanced Energy Storage Technologies Institution, Changzhou 213300, China*

† Electronic supplementary information (ESI) available. See DOI: https://doi.org/10.1039/d4sc08125k

Various electrolyte engineering designs have been applied to silicon anodes to solve the problem of slow ionic transport and excessive SEI growth. Cao *et al.* proposed a weakly solvated fully fluorinated electrolyte configured with fluoroethylene carbonate (FEC)/bis(2,2,2-trifluoromethyl) carbonate (BTFC)/ethyl trifluoroacetate (ETFA), enabling Si-based batteries to operate at a wide range of temperatures.[22] Fan's group clarified that the reduction stability of solvents is stronger with the lower electrophilicity (EPT) and coordination ability (CDA), reducing solvent decomposition for the formation of a homogeneous SEI for Li or Si anodes.[23] Zhao *et al.* reported an electrolyte based on the weak solvent cyclic tetrahydrofuran, shown to form LiF-rich interphases, achieving a long cycle life of Si anodes.[24] Furthermore, recent studies have revealed that weakly solvating electrolytes offer additional advantages, including suppressing lithium polysulfide reactivity in high-energy-density Li–S batteries and promoting the dominance of contact ion pairs and aggregates at low salt concentrations for uniform lithium deposition.[25–28] Notably, weakly solvating electrolytes have been shown to derive inorganic-rich SEI compositions suitable for silicon-based anodes to accommodate their volume changes while maintaining interfacial stability.[29–31] Advancing from these previous studies, our work proposes an appropriate and simple criterion for selecting solvents for weakly solvating electrolytes.

Here, we report an electrolyte consisting of 1.5 M lithium bis(fluorosulfonyl)imide (LiFSI) and 0.1 M lithium difluoro(oxalato)borate (LiDFOB) salt in a solvent mixture of ethyl fluoroacetate (EFA) and FEC (8 : 2 by volume) (denoted as EFA/FEC-based). This formulation exhibits weakened Li^+–solvent interaction and high lithium salt solubility, which are designed to reduce solvating ability, accelerate ionic transport, and provide F sources for forming the SEI. The weak affinity towards Li^+ promotes desolvation kinetics, and the unique anion-rich solvated structure induces earlier reduction of FSI^- to form an inorganic-rich SEI with a low resistance. As a result, the silicon–carbon (Si/C) anode is stabilized for more than 250 cycles at 0.2C in this electrolyte and retains 93.7% of its capacity after 200 cycles at 0.5C. In addition, the capacity retention of the Si/C||LFP full cell is 70.5% after 500 cycles at 0.5C. Both half and full cells exhibit dramatically improved rate performance.

2 Results and discussion

2.1 Design principle

The desolvation process of Li^+ in the electrolyte, as a pivotal factor affecting the charge transfer kinetics, determines the subsequent SEI formation and Li^+–electron binding kinetics, so reducing the desolvation energy (E_a) is the focus of our electrolyte design (Fig. 1a).[32,33] The desolvation energy is closely related to the solvation structure of the electrolyte. Theoretically, the formation of a weak solvation structure between Li^+ and solvent molecules is conducive to the desolvation process of Li^+.[4,34,35] Our strategy focuses on reducing the interaction strength between Li^+ and the solvent to significantly reduce the energy barrier for the desolvation process of the solvated Li^+,

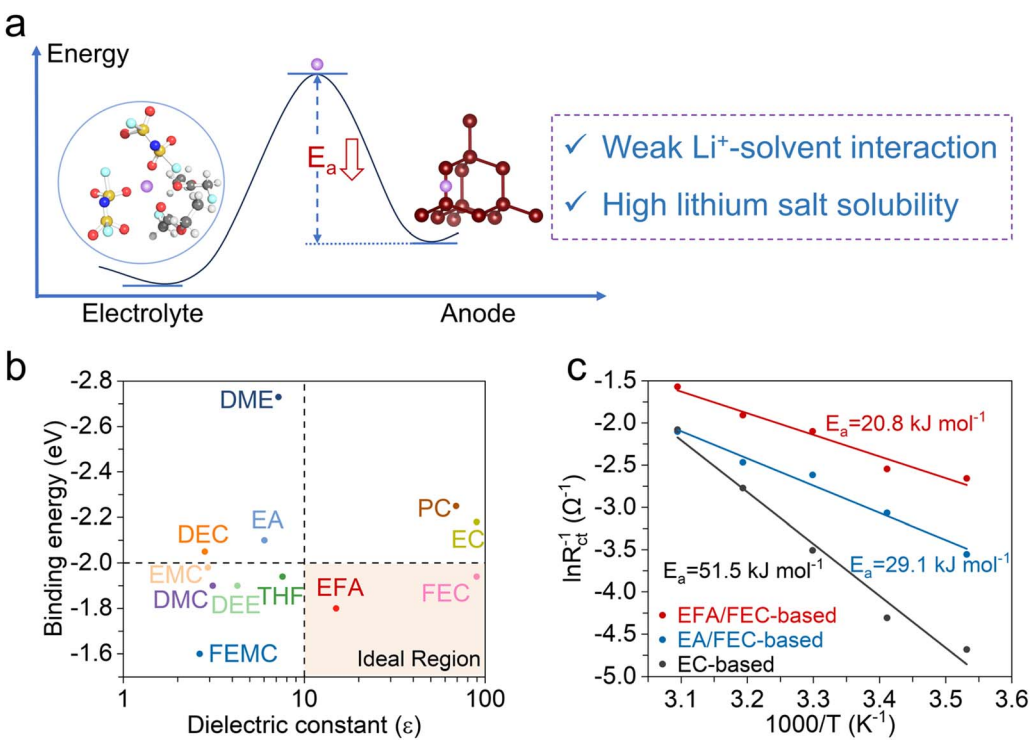

Fig. 1 Design principle of the electrolyte. (a) Schematic illustration of energetic coordinates for "Li^+ desolvation" at the silicon/electrolyte interface. (b) Diagram of binding energy and dielectric constant for solvents.[37,39] (c) Arrhenius curves and the corresponding activation energies (E_a) of the different electrolytes. EFA/FEC-based: 1.5 M LiFSI and 0.1 M LiDFOB in EFA/FEC (8 : 2, by volume). EA/FEC-based: 1.5 M LiFSI and 0.1 M LiDFOB in EA/FEC (8 : 2, by volume). EC-based: 1 M $LiPF_6$ in EC/DMC (1 : 1, by volume) with 10 wt% FEC.

which can be evaluated from the binding energy of Li^+–solvent. Simultaneously, high lithium salt solubility is required to ensure high ionic conductivity and rapid ionic transport of the electrolyte, so the solvent should have a high dielectric constant (ε). However, while a high dielectric constant promotes ionic dissociation, it also implies a strong affinity between solvent molecules and Li^+, which inhibits the desolvation process at the electrode surface and results in a low Li^+ transference number.[33]

We compare the magnitude of the dielectric constants and their binding energy to Li^+ of various common solvents in Fig. 1b. Linear carbonates are potentially attractive solvents due to their low cost, low viscosity, and low melting point. However, their dielectric constants typically range from 2 to 4, indicating a relatively weak ability to dissociate lithium salts. The linear carboxylic esters, such as ethyl acetate (EA), benefit from the low viscosities and freezing points and are often used as co-solvents to enhance the performance of LIBs at low-temperature and high rates.[36] The strong affinity (−2.1 eV) between the ester carbonyl group (C═O) and Li^+ slows down the desolvation process at the electrode/electrolyte interface.[22,37] Fluorination serves as an efficient approach to modulate the binding energy of solvents with Li^+, reducing the binding energy of EFA to −1.8 eV. The strong electron-withdrawing effect of the F atom significantly diminishes EFA's solvating ability and weakens the interactions between Li^+ and EFA.[37–39] The presence of an equilibrium region (yellow area in the lower right corner) includes solvents with low binding energy values and moderate dielectric constants, leading to moderate lithium salt dissociation while effectively reducing the affinity of Li^+ for the solvents without obstructing ionic transport.

EFA and FEC are selected as solvents for the electrolyte design based on the following considerations: (1) with adequately high dielectric constant, EFA has a favorable ability to Li^+ dissociation while its low binding energy weakens the Li^+–solvent coordination and promotes the Li^+ desolvation. (2) A small amount of FEC allows precise coordination with Li^+ to achieve a certain FEC solvation number.[40] In addition, FEC combines an appropriate binding energy and a dielectric constant value. As a co-solvent, it has a high ionic conductivity, good SEI formation ability, and high oxidation resistance.[41] (3) The coordination of Li^+–FSI^- can be strengthened, and the reduction of FSI^- occurs earlier to form an inorganic-rich SEI. The introduction of F enhances the ability to form an effective SEI on the silicon anode. The F-containing species, both organic and inorganic, are effective in the passivation of the silicon anode surface and mitigation of further electrolyte decomposition.[42] Numerous studies have shown that the LiF-rich SEI can inhibit sequential side reactions and mitigate the pulverization of active particles.[13,43] With this in mind, we used EFA and FEC for electrolyte design and determined the optimal ratio of EFA and FEC as 8 : 2 (Fig. S1a†). LiDFOB, used as a salt additive to improve cycling stability (Fig. S1b†), preferentially participates in the SEI formation during charge and discharge,[44] effectively suppressing the side reaction between the electrolyte and active materials while promoting uniform deposition of lithium metal.[45]

To evaluate the activation energy of Li^+ desolvation of electrolyte, the silicon electrodes were removed from two Li/Si cells after three activation cycles at 0.05C using the corresponding electrolytes, and then fabricated into symmetric cells for the electrochemical impedance spectra (EIS) test from 283.15 to 323.15 K. As shown in Fig. 1c and S2–S4,† due to the substantial binding energy of Li^+–EC, the E_a value of the EC-based electrolyte reaches 51.5 kJ mol^{-1}. Changing the electrolyte to EA/FEC-based, the E_a value is diminished to 29.1 kJ mol^{-1}. As expected, the substitution of EFA solvent reduces the E_a to 20.8 kJ mol^{-1}, attributed to the lower binding energy of the Li^+–EFA reducing the Li^+–solvent interaction in the solvation shell, which speeds up the desolvation process.

The conductivity of the electrolytes compared in Fig. S5† shows that the EFA/FEC-based electrolyte is endowed with a high conductivity at room temperature (10.55 mS cm^{-1}), the same level as the EC-based electrolyte (11.32 mS cm^{-1}). What really matters for the performance of batteries is the Li^+ migration, and the high conductivity does not directly equate to high efficiency of Li^+ migration. Li/Li symmetric batteries were polarized at a constant potential of 10 mV, and the values of Li^+ transference numbers (t_{Li^+}) of EC-based, EA/FEC-based, and EFA/FEC-based electrolytes are 0.15, 0.55, and 0.67, respectively (Fig. 2a and Table S1†). A low Li^+ transference number will form concentrated differential polarization during the cycling process of the battery, especially at high rates. According to the results, the diffusion of Li^+ in the electrolyte is accelerated due to the low viscosity of small EA molecules. When replacing EA with EFA, the t_{Li^+} was substantially increased, attributed to the low viscosity EFA inherited from EA and the reduced shielding effect on Li^+ due to the reduction of solvent molecules.[39]

2.2 Solvation structures of electrolytes

The solvation structures of the electrolytes described above were further studied using Fourier transform infrared (FT-IR) spectroscopy. Fig. 2b presents the FT-IR spectra of the carboxylic ester carbonyl group (C═O) in pure EA, pure EFA, LiFSI–EA, and LiFSI–EFA. The peak near 1736 cm^{-1} is related to the free EA molecules, whereas the peak at about 1704 cm^{-1} is associated with the coordination of Li^+–EA in LiFSI–EA. Likewise, the pure EFA solvent exhibits the characteristic stretching vibration of C═O, with an additional peak at approximately 1770 cm^{-1}, possibly resulting from Fermi resonance, and the peak at 1763 cm^{-1} is attributed to the free EFA.[38,46] Fluorination induces a shift of the C═O stretching vibration to a higher wavenumber, and new peaks appearing at lower wavenumbers correspond to Li^+ coordinated solvents (Fig. S6†). The much weaker peak of Li^+–EFA coordination at 1716 cm^{-1} compared to Li^+–EA coordination indicates that the Li^+–solvent interaction is significantly reduced. Fig. 2c and d show the Raman spectra of EA, EFA, FEC, and electrolytes. The FSI^- anion of the EFA/FEC-based electrolyte has the strongest interaction with Li^+, as evidenced by the S–N–S stretching vibration of FSI^- at 733.7 cm^{-1}, which has the smallest redshift relative to that in the LiFSI salt (774 cm^{-1}).[47] Raman spectra fitting results reveal that free anions (SSIP, uncoordinated to Li^+), contact-ion-pairs (CIP, one

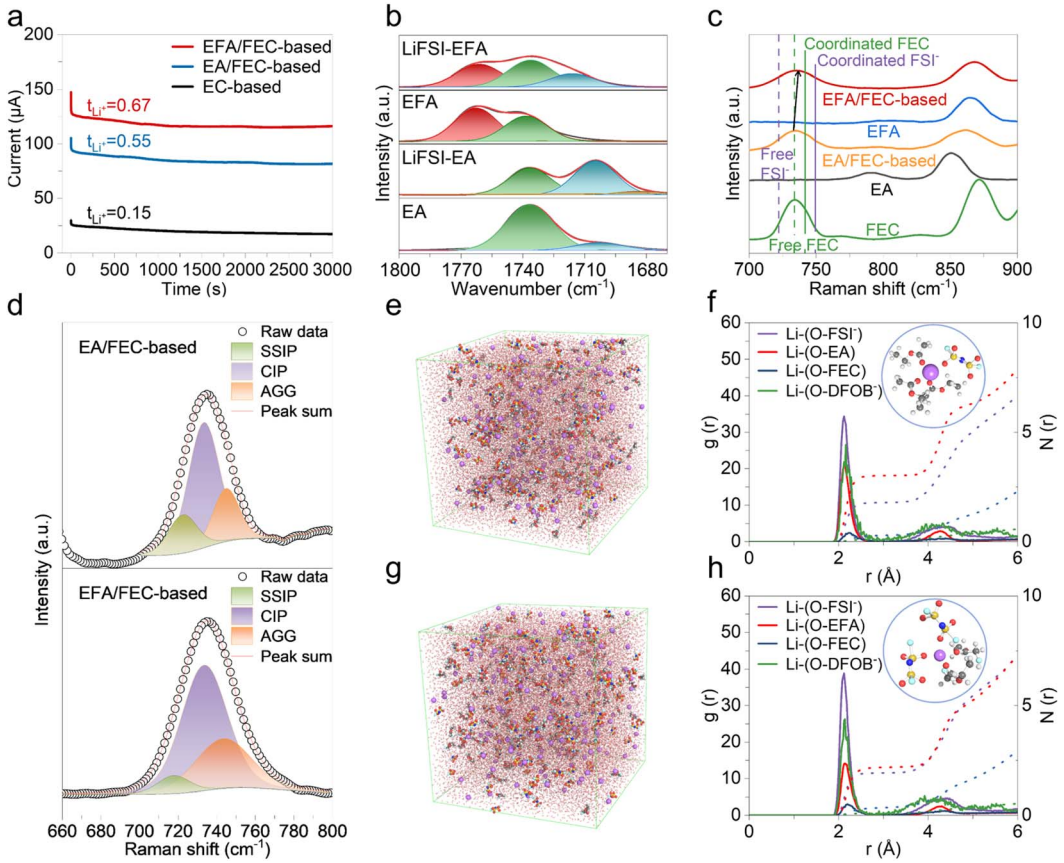

Fig. 2 Solvation structure of electrolytes. (a) *I*–*t* curves of the cells with different electrolytes. (b) FT-IR spectra of C=O in EA, EFA, LiFSI–EA (1.5 M LiFSI in EA), and LiFSI–EFA (1.5 M LiFSI in EFA). (c) Raman spectra of the FEC, EA, EFA, and electrolytes. (d) Fitting results of the Raman spectra of the EA/FEC-based and EFA/FEC-based electrolytes in the range from 660 to 800 cm^{-1}. MD snapshots of (e) EA/FEC-based and (g) EFA/FEC-based electrolytes. The radial distribution function and coordination number of (f) EA/FEC-based and (h) EFA/FEC-based electrolytes. The oxygen atoms in EA, EFA, FEC, FSI$^-$ and DFOB$^-$ are denoted as O–EA, O–EFA, O–FEC, O–FSI$^-$ and O–DFOB$^-$, respectively. And the corresponding illustrations are the typical solvation structures of electrolytes in the primary Li$^+$ solvation shell, in which the atoms are represented by balls of different colors (H: white, Li: purple, B: pink, C: grey, N: blue, O: red, F: light blue, S: yellow).

FSI$^-$ anion coordinating to one Li$^+$), and aggregates (AGG, one FSI$^-$ anion coordinating to more than two Li$^+$) of the solvated structure in the EFA/FEC-based electrolyte accounted for 6.31%, 63.24%, and 30.45%, respectively. The number of coordinated FSI$^-$ is increased compared to that of the EA/FEC-based electrolyte, and the corresponding peaks of the free solvent molecules are significantly weakened, indicating that more solvent molecules are involved in the Li$^+$ solvation shell.

Molecular dynamics (MD) simulations further confirmed the spectral analysis results. The simulated results are shown in Fig. 2e–h and S7.† For the EA/FEC-based electrolyte, the average coordination number of EA is 3.017, whereas that of FSI$^-$ is only 1.780, indicating that the EA solvent is dominant in the solvation shell. As the illustration in Fig. 2f shows, the representative solvation structure in the EA/FEC-based electrolyte is one FSI$^-$ and three EA coordinating with Li$^+$. The high binding energy of Li$^+$–EA significantly increases the barrier for Li$^+$ desolvation. The $g(r)$ value of the Li–O_{FSI^-} pair increases obviously, and the Li–O_{EFA} peak significantly decreases, suggesting that the FSI$^-$ participates more extensively in the primary Li$^+$ solvation shell, which is the result of the reduced ionic-dipole interactions of Li$^+$–EFA.[22] The illustration in Fig. 2h shows that the representative solvation structure in the EFA/FEC-based electrolyte is two FSI$^-$ and two EFA coordinating with Li$^+$. Accordingly, the coordination number of the EFA decreases to 2.183, and that of FSI$^-$ increases to 1.921 in the EFA/FEC-based electrolyte, indicating that the coordination interaction of Li$^+$–FSI$^-$ is enhanced. According to the results of calculations, the anionic content within the solvation structure of Li$^+$ in the EFA/FEC-based electrolyte increased from 24.1% to 31.3% compared to that of the EA/FEC-based electrolyte (Fig. S7†). The high level of anions in the solvated structure facilitates the formation of CIP and AGG, which is conducive to constructing a stable and robust interphase.[48,49]

2.3 Electrochemical performance of Si/C anodes

The charge/discharge profiles of Si/C anodes are compared in Fig. 3a–c, using Li/Si cells at a rate of 0.2C (1C = 1800 mA g^{-1}). In contrast to the other two, lower polarization is observed in the EFA/FEC-based electrolyte. The initial discharge capacities with the EC-based, EA/FEC-based, and EFA/FEC-based electrolytes are 1903.3, 2038.4, and 2085.3 mAh g^{-1}, respectively,

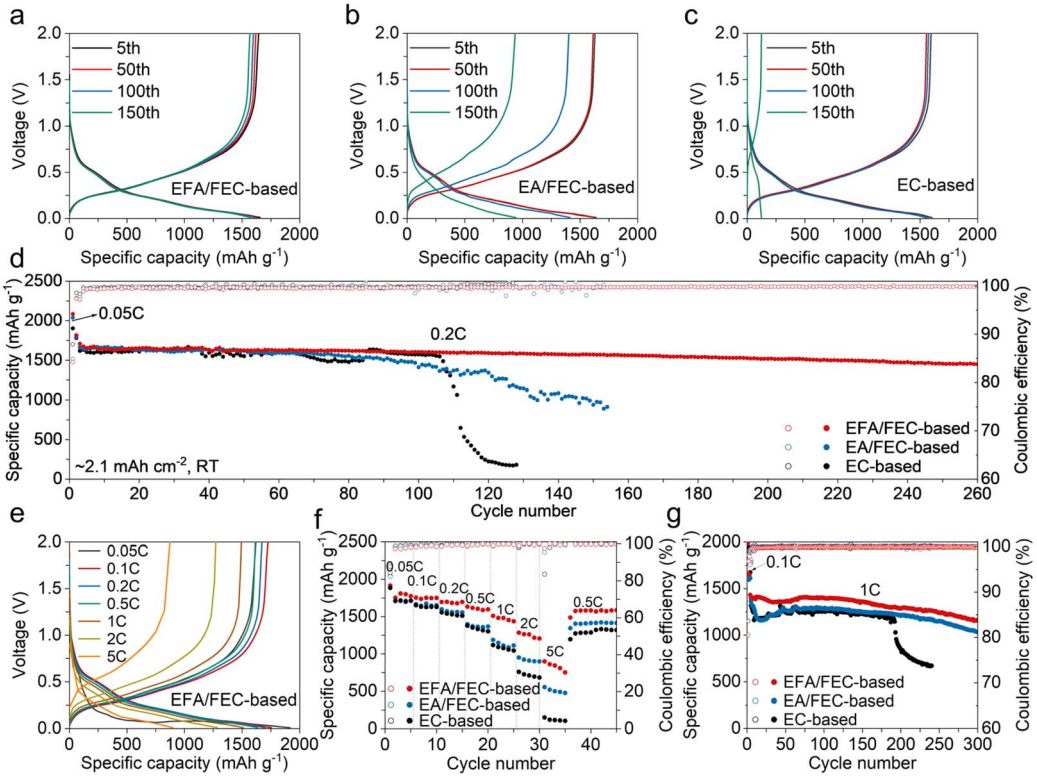

Fig. 3 Electrochemical performance of Li/Si cells with the three electrolytes. Corresponding charge/discharge voltage profiles of Li/Si cells using (a) EFA/FEC-based, (b) EA/FEC-based, and (c) EC-based electrolytes. (d) Cycling performance at 0.2C after two activation cycles at 0.05C. (e) Charge/discharge curves at different rates using the EFA/FEC-based electrolyte. (f) Rate performance using the three electrolytes. (g) Cycling performance at 1C after three activation cycles at 0.1C.

corresponding to the initial Coulombic efficiency (ICE) of 87.1%, 85.5%, and 86.3%, respectively (Fig. S8†). The morphology and composition of the Si/C materials are revealed in Fig. S9–S11.† To investigate the delithiation/lithiation behavior of Si/C anodes, cyclic voltammetry (CV) was carried out. As shown in Fig. S12,† the reduction peak observed below 0.05 V signifies the initial lithiation process of the active crystalline Si to form Li_xSi, which splits into two peaks at 0.47 and 0.02 V in subsequent cycles, indicating amorphization of the Si/C anode. Meanwhile, the oxidation peaks of silicon corresponding to dealloying were assigned at 0.35 and 0.50 V during the positive scan.[10,50,51] With cycling at 0.2C to over 100 cycles, the difference in capacity between the batteries using different electrolytes begins to show up clearly. Specifically, only a low discharge capacity of 223.3 mAh g^{-1} in the Li/Si cells using the EC-based electrolyte was retained after 120 cycles. Sharp capacity decay exhibits a typical result when using conventional EC-based carbonate electrolytes, as the organic SEIs derived from carbonates fail to efficiently suppress volume changes.[20] The Si/C anodes in the EA/FEC-based electrolyte exhibit improved cycling performance (Fig. 3d) but still suffer from a continuous capacity drop. After 150 cycles, the discharge capacity decreased to 941.1 mAh g^{-1}, with a remaining capacity of only 56.6%. Further replacing the EA in the EA/FEC-based electrolyte with EFA solvent resulted in improved cycling stability, achieving a discharge capacity of 1572.4 mAh g^{-1} and a capacity retention of 92.0% after 150 cycles. Half cells in EFA/FEC-based electrolyte run steadily for more than 260 cycles and retain 84.9% of the initial capacity (1709.1 mAh g^{-1} at 0.2C).

The rate performance of the Si/C anodes was assessed between 0.05C and 5C. As indicated in Fig. 3e and f, Si/C anodes using the EC-based electrolyte deliver almost no capacity at a discharge rate of 5C. It can be observed that the cell based on the EA/FEC-based electrolyte provides significantly higher discharge capacities of 952.1 and 550.0 mAh g^{-1} at 2C and 5C, respectively. As expected, the Si/C anodes using the EFA/FEC-based electrolyte display an excellent rate capability compared with others, further increasing discharge capacities to 1284.7 and 900.0 mA h g^{-1} at 2C and 5C, respectively. Meanwhile, the EFA/FEC-based cells can obtain a high reversible capacity of 1311.2 mAh g^{-1} after 200 cycles of stable cycling at 0.5C (Fig. S13†), demonstrating a high retention rate of 93.7%. By comparison, the control with the EC-based electrolyte shows a rapid capacity decay, and EA/FEC-based cells deliver 1139.3 mA h g^{-1} with only 81.6% of their capacity retained after 200 cycles at 0.5C. Furthermore, at a higher rate of 1C (Fig. 3g), the cell with the EFA/FEC-based electrolyte exhibits a high specific capacity of 1433.6 mAh g^{-1} at the 4th cycle, with a capacity retention of 81.15% after 300 cycles. The cycling performance of the cells using the EFA/FEC-based electrolyte is compared with other published studies in Table S2,† demonstrating its superiority and high compatibility with silicon anodes.

2.4 Interfacial properties of the cycled electrodes

The data from EIS may partially reveal the reason for the difference in cycling stability and rate capability using the three electrolytes. As shown in Fig. 4a and S14a,† EC-based cells exhibit a maximum charge transfer impedance (R_{ct}) of 121.3 Ω, while the cells with the EFA/FEC-based electrolyte show the smallest impedance of 30.08 Ω before cycling. After the first cycle, the R_{ct} of all three electrolytes tends to decrease since the expansion and contraction of silicon leads to a much more complete contact between the electrode and the electrolyte.[34] However, the R_{ct} of the cells with the EC-based electrolyte shows an increasing trend after 50 cycles, indicating deteriorated lithiation/delithiation kinetics on the electrodes, which is caused by the continuously increasing thickness of the SEI during cycling. This can still be confirmed from the values of R_{SEI} after 50 cycles in Fig. S14b,† and the SEI developed in the EFA/FEC-based electrolyte presents the minimal impedance of 2.16 Ω, suggesting that the less resistive SEIs are susceptible to Li^+ migration. In summary, the Li^+ migration energy barrier in the EFA/FEC-based electrolyte is relatively low, and the Li^+ desolvation energy is decreased, which leads to the acceleration of Li^+ desolvation kinetics. Furthermore, the SEI film in the EFA/FEC-based electrolyte has a higher ionic conductivity, which speeds up the migration of Li^+ through the SEI.[23]

The impedance of Li^+ across the SEI is strongly correlated with the thickness and chemical compositions of the interphase, as revealed by transmission electron microscopy (TEM) and X-ray photoelectron spectroscopy (XPS) characterization studies. TEM images of silicon electrodes after 50 cycles in different electrolytes are shown in Fig. 4b. After cycling in the EC-based electrolyte, a rather thick and inhomogeneous SEI of about 50 nm was obtained due to the continuous accumulation of by-products. When using the EFA/FEC-based electrolyte, the SEI shows a thickness of 14–18 nm, which was relatively thinner than that obtained using the other two electrolytes. The thin SEI facilitates the diffusion of Li^+ and shortens the path for Li^+ transport,[40] contributing to enhanced rate performance of the Si/C anode in the EFA/FEC-based electrolyte. The disparity in thickness in these three electrolytes is intimately related to the

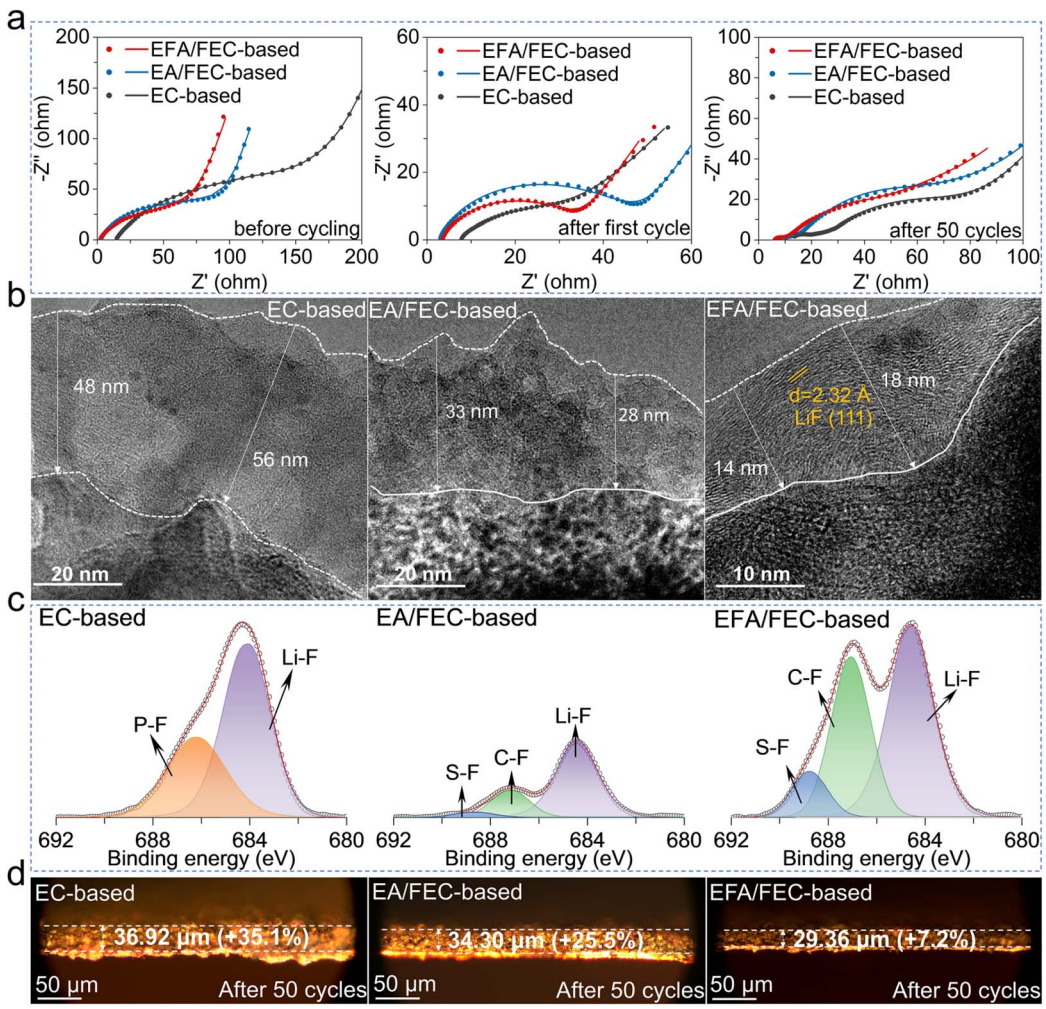

Fig. 4 Interfacial characterization of the cycled Si/C anodes. (a) EIS of Li/Si cells in corresponding electrolytes and their fitting results at different periods; the points represent the raw data, and the lines represent the fitting data. (b) TEM images of the Si/C anodes after 100 cycles. (c) The XPS spectra of F 1s of Si/C anodes after 100 cycles. (d) Optical images of the cross-section of the Si/C anodes after 50 cycles.

chemical constitution of the formed SEI. To explore the reasons behind the superior electrochemical performance of the Si/C anode in the EFA/FEC-based electrolyte, the formation of the SEI after 100 cycles was investigated by the XPS technique. Notably, the addition of FEC significantly promoted LiF formation in the EC-based phase. For EA/FEC-based and EFA/FEC-based electrolytes, the F 1s spectra (Fig. 4c) show inorganic species containing S–F, C–F, and Li–F bonds.[38,42] However, the higher-strength LiF signal and the lattice fringes of LiF (111) can be observed from the interphase layer established with the EFA/FEC-based electrolyte in Fig. 4b and c. The *in situ* growth of the LiF-rich SEI layer is conducive to high Li^+ conductivity, typically attributed to its large bandgap, high shear modulus, and electronic insulation properties.[22,52] The gradual increase in C–F and S–F content in the EFA/FEC-based electrolyte resulting from the decomposition of FSI^- can be detected, well demonstrating the weak affinity of Li^+–solvent and the involvement of more anions in the solvation structure.

The C 1s and O 1s spectra exhibit major peaks attributed to CO_3^{2-}, C–O, and C=O substances (Fig. S15a and b†).[53] In contrast, these typical signals associated with organic substances are significantly weaker when using the EFA/FEC-based electrolyte. The inorganic crystalline LiF-dominated SEI possesses higher interfacial energy and weaker bonding to the Li–Si alloy, ensuring its integrity during large volume changes of the internal Li_xSi.[42,43] The organic-rich SEI formed in the EC-based electrolyte has lower interfacial energy and stronger bonding to the alloy phase, which will rupture during volume deformation of the alloy phase, leading to an electrolyte penetration and a rapid capacity degradation.[20,53] The higher content of sulfur components (S–F, $-SO_xF$, Fig. 4c and S15c†) on the surface is due to the decomposition of the FSI^- anion, which results in the participation of more anions in the solvated sheath layer.[38,54] The electrolyte promotes the formation of the SEI with inorganic-rich components on the Si/C anode, which features a low electronic conductivity as well as the ability to conduct Li^+ rapidly. The inorganic-rich SEI exhibits low thickness, leading to minimal resistance, which facilitates rapid Li^+ migration across the interfacial phase. The easy Li^+ desolvation process and the subsequent rapid ionic motion through the SEI can effectively explain the superior performance of Si/C anodes in the EFA/FEC-based electrolyte.

Optical microscopy was employed to observe the efficacy of the SEI in different electrolytes to withstand the volume changes of the cycled electrodes. The enhanced stability of the inorganic LiF-rich SEI in comparison to the organic SEI is further evidenced by the suppressed growth of the thickness of the electrode after 50 cycles in electrolytes. As shown in Fig. 4d and S16,† the electrode thickness is 27.33 μm before cycling and 29.36 μm after 50 cycles in the EFA/FEC-based electrolyte, with an expansion rate of 7.2%, which shows the smallest increase in thickness compared to 35.1% in EC-based electrolyte and 25.5% in EA/FEC-based electrolyte. The extremely low increase in the thickness of the electrodes in the EFA/FEC-based electrolyte is much lower than that reported in other studies.[55,56] It proves the superior mechanical properties of the generated inorganic LiF-rich SEI film and emphasizes the essential role of the EFA/FEC-based electrolyte in mitigating the inherent volume change challenges in silicon-based anodes, thereby contributing to improved electrochemical performance.

2.5 Electrochemical performance of Si/C||LFP full cells

The full cell consists of a Si/C anode paired with a commercial LFP cathode, and the Si/C anode was pre-lithiated with an N/P ratio of 1.12 before cycling. Combined with the exploration of the solvation structures and the interphases, it can be inferred

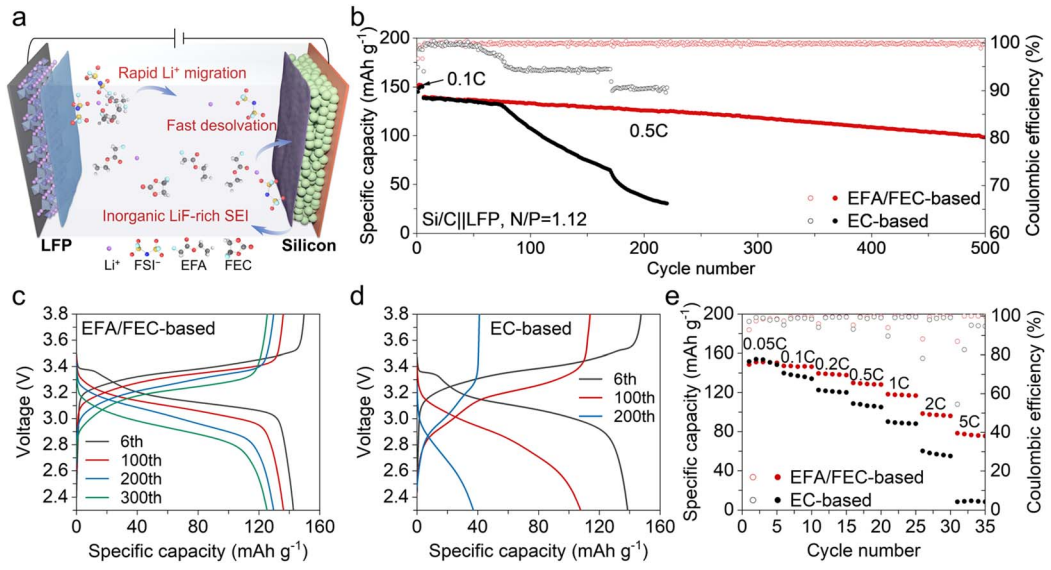

Fig. 5 Electrochemical performance of Si/C||LFP cells at room temperature. (a) Schematic illustration of interfacial Li^+ transport kinetics and interfacial stability of the Si/C||LFP battery. (b) Cycling performance at 0.5C after five activation cycles at 0.05C (1C = 170 mA g^{-1}). Corresponding charge/discharge curves of Si/C||LFP cells using (c) EFA/FEC-based and (d) EC-based electrolytes. (e) Rate performance using EFA/FEC-based and EC-based electrolytes.

that the rapid migration of Li^+ in the electrolyte, the fast desolvation process, and the low resistance of SEI can be effectively achieved by rationally adjusting the solvent molecules to ensure the easy movement of Li^+ at the interface, as illustrated in Fig. 5a. The full cells with the EFA/FEC-based electrolyte exhibit stable cycling, and the cycling performance of the Si/C||LFP full cells is shown in Fig. 5b. As expected, the EC-based electrolyte does not support reversible cycling of the cells, with the capacity fading rapidly and only 26.8% capacity retention after 200 cycles. Due to the dramatic volume changes and the unstable SEI, a severe SEI build-up and a degradation of the electrode structure occur in the EC-based electrolyte. In contrast, by employing the EFA/FEC-based electrolyte, the capacity retention after 200 cycles has been increased to 90.2%, and the cell retains 70.5% of its original capacity after 500 cycles.

The limited voltage polarization during the cycling process, shown in Fig. 5c and d, indicates stable electrodes and easy Li^+ transport. In addition to excellent cycling performance, the EFA/FEC-based electrolyte exhibits remarkable effectiveness in improving the rate performance of Si/C||LFP cells. As seen in Fig. 5e and S17,† the full cell with the EC-based electrolyte shows great polarization, with a low capacity retention of 55.4% at 2C and only 8.7% at 5C compared to the capacity at 0.5C. There is a significant increase in the discharge capacity using the EFA/FEC-based electrolyte at different rates, corresponding to a rising capacity retention of 75.8% at 2C and 60.4% at 5C compared to the capacity at 0.5C.

3 Conclusions

In summary, *via* electrolyte solvation engineering, we have successfully explored and designed EFA and FEC as co-solvents to enhance ionic transport and mitigate excessive SEI growth on Si anodes. Efficaciously weakened Li^+–solvent binding knocks down the Li^+ desolvation barrier. The preferential decomposition of the FSI^- anion alters SEI formation, endowing it with abundant LiF and other inorganic substances. As a result, the formation of the fluorine-rich electrolyte/electrode interphase passivates the Si/C electrode, preventing successive solvent reduction and structural collapse. Benefitting from the high ionic conductivity (10.55 mS cm^{-1}), a high Li^+ transference number (0.67), the rapid desolvation process realized by the weak Li^+–EFA solvation interactions, and low resistance of Li^+ diffusion across the SEI, the Li/Si half cells display excellent cycling stability and fast-charging capability up to 5C (900.0 mAh g^{-1}). The Si/C||LFP full cells achieve stable cycling of over 500 cycles, significantly outperforming cells using conventional EC-based electrolytes. The design strategy proposed in this study is considered to offer valuable guidance for advancing fast-charging and long-cycling Si-based battery systems.

Data availability

The data supporting this article have been included as part of the ESI.†

Author contributions

Min Li: investigation, data curation, validation, visualization, formal analysis, writing – original draft, writing – review & editing. Shuai Li: methodology, investigation, writing – review & editing. Dong Yan: investigation, writing – review & editing. Yuhao Ma: visualization, writing – review & editing. Xiaobin Niu: writing – review & editing. Liping Wang: conceptualization, supervision, writing-review & editing, funding acquisition.

Conflicts of interest

There are no conflicts to declare.

Acknowledgements

This work was supported by the National Natural Science Foundation of China (No. 22322903 and 52072061), the Natural Science Foundation of Sichuan, China (No. 2023NSFSC1914), and Beijing National Laboratory for Condensed Matter Physics (2023BNLCMPKF015).

Notes and references

1 Y. Li, Y. Zheng, K. Guo, J. Zhao and C. Li, Mg-Li Hybrid Batteries: The Combination of Fast Kinetics and Reduced Overpotential, *Energy Mater. Adv.*, 2022, **2022**, 9840837.
2 X. Fan, M. Tebyetekerwa, Y. Wu, R. R. Gaddam and X. S. Zhao, Magnesium/Lithium Hybrid Batteries Based on SnS_2-MoS_2 with Reversible Conversion Reactions, *Energy Mater. Adv.*, 2022, **2022**, 9846797.
3 Q. K. Zhang, X. Q. Zhang, L. P. Hou, S. Y. Sun, Y. X. Zhan, J. L. Liang, F. S. Zhang, X. N. Feng, B. Q. Li and J. Q. Huang, Regulating Solvation Structure in Nonflammable Amide-Based Electrolytes for Long-Cycling and Safe Lithium Metal Batteries, *Adv. Energy Mater.*, 2022, **12**, 2200139.
4 L. Luo, K. Chen, R. Cao, H. Chen, M. Xia, A. Zhao, X. Chen, W. Chen, Z. Chen, Y. Fang and Y. Cao, Ethyl Fluoroacetate with Weak Li^+ Interaction and High Oxidation Resistant Induced Low-Temperature and High-Voltage Graphite//$LiCoO_2$ Batteries, *Energy Storage Mater.*, 2024, **70**, 103438.
5 Z. Li, G. Zhou, S. Li, H. Liu, L. Wang and H. Li, Unlocking Cycling Longevity in Micro-Sized Conversion-Type FeS_2 Cathodes, *Joule*, 2023, **7**, 2609–2621.
6 H. Liu, Z. Wu, H. Wang, X. Niu, H. Li and L. Wang, Chelating-Type Binders toward Stable Cycling and High-Safety Transition-Metal Sulfide-Based Lithium Batteries, *ACS Energy Lett.*, 2024, **9**, 4666–4672.
7 L. Wang, Z. Wu, J. Zou, P. Gao, X. Niu, H. Li and L. Chen, Li-Free Cathode Materials for High Energy Density Lithium Batteries, *Joule*, 2019, **3**, 2086–2102.
8 B. Li, Z. Zhuo, L. Zhang, A. Iadecola, X. Gao, J. Guo, W. Yang, A. V. Morozov, A. M. Abakumov and J.-M. Tarascon, Decoupling the Roles of Ni and Co in Anionic Redox Activity of Li-Rich NMC Cathodes, *Nat. Mater.*, 2023, **22**, 1370–1379.

9 W.-J. Kong, C.-Z. Zhao, L. Shen, S. Sun, X.-Y. Huang, P. Xu, Y. Lu, W.-Z. Huang, J.-L. Li, J.-Q. Huang and Q. Zhang, Bulk/Interfacial Structure Design of Li-Rich Mn-Based Cathodes for All-Solid-State Lithium Batteries, *J. Am. Chem. Soc.*, 2024, **146**, 28190–28200.
10 K. Feng, M. Li, W. Liu, A. G. Kashkooli, X. Xiao, M. Cai and Z. Chen, Silicon-Based Anodes for Lithium-Ion Batteries: From Fundamentals to Practical Applications, *Small*, 2018, **14**, 1702737.
11 L. Yang, T. Meng, W. Zheng, J. Zhong, H. Cheng, Y. Tong and D. Shu, Advanced Binder Design for High-Performance Silicon Anodes, *Energy Storage Mater.*, 2024, **72**, 103766.
12 F. Shi, Z. Song, P. N. Ross, G. A. Somorjai, R. O. Ritchie and K. Komvopoulos, Failure Mechanisms of Single-Crystal Silicon Electrodes in Lithium-Ion Batteries, *Nat. Commun.*, 2016, **7**, 11886.
13 Y. Yang, J. Wang, Z. Li, Z. Yang, B. Wang and H. Zhao, Constructing LiF-Dominated Interphases with Polymer Interwoven Outer Layer Enables Long-Term Cycling of Si Anodes, *ACS Nano*, 2024, **18**, 7666–7676.
14 Y.-C. Yen, S.-C. Chao, H.-C. Wu and N.-L. Wu, Study on Solid-Electrolyte-Interphase of Si and C-Coated Si Electrodes in Lithium Cells, *J. Electrochem. Soc.*, 2009, **156**, A95–A102.
15 Z. Wang, Z. Sun, Y. Shi, F. Qi, X. Gao, H. Yang, H. M. Cheng and F. Li, Ion-Dipole Chemistry Drives Rapid Evolution of Li Ions Solvation Sheath in Low-Temperature Li Batteries, *Adv. Energy Mater.*, 2021, **11**, 2100935.
16 K. Xu, A. von Cresce and U. Lee, Differentiating Contributions to "Ion Transfer" Barrier from Interphasial Resistance and Li^+ Desolvation at Electrolyte/Graphite Interface, *Langmuir*, 2010, **26**, 11538–11543.
17 G. Song, Z. Yi, F. Su, L. Xie, Z. Wang, X.-X. Wei, G. Xu and C.-M. Chen, Boosting the Low-Temperature Performance for Li-Ion Batteries in $LiPF_6$-Based Local High-Concentration Electrolyte, *ACS Energy Lett.*, 2023, **8**, 1336–1343.
18 T. Ma, Y. Ni, Q. Wang, W. Zhang, S. Jin, S. Zheng, X. Yang, Y. Hou, Z. Tao and J. Chen, Optimize Lithium Deposition at Low Temperature by Weakly Solvating Power Solvent, *Angew. Chem., Int. Ed.*, 2022, **61**, e202207927.
19 Z. Wang, Y. Wang, Y. Xin, Q. Zhou, X. Ding, L. Liu, T. Song, F. Wu, Z. Wei and H. Gao, Simultaneous Modulation of Cathode/Anode and Electrolyte Interfaces Via a Nitrile Additive for High-Energy-Density Lithium-Metal Batteries, *Chem. Sci.*, 2024, **15**, 16669–16680.
20 Y. Zhai, Z. Zhong, N. Kuang, Q. Li, T. Xu, J. He, H. Li, X. Yin, Y. Jia, Q. He, S. Wu and Q. H. Yang, Both Resilience and Adhesivity Define Solid Electrolyte Interphases for a High Performance Anode, *J. Am. Chem. Soc.*, 2024, **146**, 15209–15218.
21 S. Park, S. Kim, J. A. Lee, M. Ue and N. S. Choi, Liquid Electrolyte Chemistries for Solid Electrolyte Interphase Construction on Silicon and Lithium-Metal Anodes, *Chem. Sci.*, 2023, **14**, 9996–10024.
22 Z. Cao, X. Zheng, M. Zhou, T. Zhao, L. Lv, Y. Li, Z. Wang, W. Luo and H. Zheng, Electrolyte Solvation Engineering toward High-Rate and Low-Temperature Silicon-Based Batteries, *ACS Energy Lett.*, 2022, **7**, 3581–3592.
23 C. Sun, R. Li, S. Weng, C. Zhu, L. Chen, S. Jiang, L. Li, X. Xiao, C. Liu, L. Chen, T. Deng, X. Wang and X. Fan, Reduction-Tolerance Electrolyte Design for High-Energy Lithium Batteries, *Angew. Chem., Int. Ed.*, 2024, **63**, e202400761.
24 Y. Yang, Z. Yang, Z. Li, J. Wang, X. He and H. Zhao, Rational Electrolyte Design for Interfacial Chemistry Modulation to Enable Long-Term Cycling Si Anode, *Adv. Energy Mater.*, 2023, **13**, 2302068.
25 X.-Y. Li, S. Feng, Y.-W. Song, C.-X. Zhao, Z. Li, Z.-X. Chen, Q. Cheng, X. Chen, X.-Q. Zhang, B.-Q. Li, J.-Q. Huang and Q. Zhang, Kinetic Evaluation on Lithium Polysulfide in Weakly Solvating Electrolyte toward Practical Lithium-Sulfur Batteries, *J. Am. Chem. Soc.*, 2024, **146**, 14754–14764.
26 T. Ma, Y. Ni, Q. Wang, W. Zhang, S. Jin, S. Zheng, X. Yang, Y. Hou, Z. Tao and J. Chen, Optimize Lithium Deposition at Low Temperature by Weakly Solvating Power Solvent, *Angew. Chem., Int. Ed.*, 2022, **61**, e202207927.
27 H. Zhang, Z. Zeng, F. Ma, Q. Wu, X. Wang, S. Cheng and J. Xie, Cyclopentylmethyl Ether, a Non-Fluorinated, Weakly Solvating and Wide Temperature Solvent for High-Performance Lithium Metal Battery, *Angew. Chem., Int. Ed.*, 2023, **62**, e202300771.
28 Y. X. Yao, X. Chen, C. Yan, X. Q. Zhang, W. L. Cai, J. Q. Huang and Q. Zhang, Regulating Interfacial Chemistry in Lithium-Ion Batteries by a Weakly Solvating Electrolyte, *Angew. Chem., Int. Ed.*, 2020, **60**, 4090–4097.
29 S. He, S. Huang, X. Liu, X. Zeng, H. Chen, L. Zhao, H. Noor and X. Hou, Electrolyte Design for Robust Gradient Solid-Electrolyte Interfaces to Enable High-Performance Silicon Anodes for Pouch Batteries, *Chem. Eng. J.*, 2024, **489**, 150620.
30 X. Peng, B. Liu, J. Chen, Q. Jian, Y. Li and T. Zhao, A Steric-Hindrance-Induced Weakly Solvating Electrolyte Boosting the Cycling Performance of a Micrometer-Sized Silicon Anode, *ACS Energy Lett.*, 2023, **8**, 3586–3594.
31 W. Chen, D. Zhang, H. Fu, J. Li, X. Yu, J. Zhou and B. Lu, Restructuring Electrolyte Solvation by a Partially and Weakly Solvating Cosolvent toward High-Performance Potassium-Ion Batteries, *ACS Nano*, 2024, **18**, 12512–12523.
32 J. Holoubek, H. Liu, Z. Wu, Y. Yin, X. Xing, G. Cai, S. Yu, H. Zhou, T. A. Pascal, Z. Chen and P. Liu, Tailoring Electrolyte Solvation for Li Metal Batteries Cycled at Ultra-Low Temperature, *Nat. Energy*, 2021, **6**, 303–313.
33 Y. Chen, Q. He, Y. Zhao, W. Zhou, P. Xiao, P. Gao, N. Tavajohi, J. Tu, B. Li, X. He, L. Xing, X. Fan and J. Liu, Breaking Solvation Dominance of Ethylene Carbonate Via Molecular Charge Engineering Enables Lower Temperature Battery, *Nat. Commun.*, 2023, **14**, 8326.
34 S. Li, H. Liu, L. Zheng, C. Ma, H. Yu, X. Wu, X. Niu and L. Wang, Electrolyte with Weakly Coordinating Solvents for High-Performance FeS_2 Cathode, *Nano Energy*, 2024, **131**, 110234.
35 Y. Chen, S. L. Liao, H. Gong, Z. Zhang, Z. Huang, S. C. Kim, E. Zhang, H. Lyu, W. Yu, Y. Lin, P. Sayavong, Y. Cui, J. Qin and Z. Bao, Hyperconjugation-Controlled Molecular Conformation Weakens Lithium-Ion Solvation and

Stabilizes Lithium Metal Anodes, *Chem. Sci.*, 2024, **15**, 19805–19819.

36 X. Dong, Y. Lin, P. Li, Y. Ma, J. Huang, D. Bin, Y. Wang, Y. Qi and Y. Xia, High-Energy Rechargeable Metallic Lithium Battery at −70 °C Enabled by a Cosolvent Electrolyte, *Angew. Chem., Int. Ed.*, 2019, **58**, 5623–5627.

37 Y. Wu, Q. Hu, H. Liang, A. Wang, H. Xu, L. Wang and X. He, Electrostatic Potential as Solvent Descriptor to Enable Rational Electrolyte Design for Lithium Batteries, *Adv. Energy Mater.*, 2023, **13**, 2300259.

38 Y. Mo, G. Liu, Y. Yin, M. Tao, J. Chen, Y. Peng, Y. Wang, Y. Yang, C. Wang, X. Dong and Y. Xia, Fluorinated Solvent Molecule Tuning Enables Fast-Charging and Low-Temperature Lithium-Ion Batteries, *Adv. Energy Mater.*, 2023, **13**, 2301285.

39 Y. Wang, Z. Li, Y. Hou, Z. Hao, Q. Zhang, Y. Ni, Y. Lu, Z. Yan, K. Zhang, Q. Zhao, F. Li and J. Chen, Emerging Electrolytes with Fluorinated Solvents for Rechargeable Lithium-Based Batteries, *Chem. Soc. Rev.*, 2023, **52**, 2713–2763.

40 Z. Cao, X. Zheng, Q. Qu, Y. Huang and H. Zheng, Electrolyte Design Enabling a High-Safety and High-Performance Si Anode with a Tailored Electrode-Electrolyte Interphase, *Adv. Mater.*, 2021, **33**, 2103178.

41 H. Ren, G. Zheng, Y. Li, S. Chen, X. Wang, M. Zhang, W. Zhao, H. Yi, W. Huang, J. Fang, T. Liu, L. Yang, M. Liu, Q. Zhao and F. Pan, Stabilizing $LiCoO_2$ at 4.6 V by Regulating Anti-Oxidative Solvents, *Energy Environ. Sci.*, 2024, **17**, 7944–7957.

42 J. Chen, X. Fan, Q. Li, H. Yang, M. R. Khoshi, Y. Xu, S. Hwang, L. Chen, X. Ji, C. Yang, H. He, C. Wang, E. Garfunkel, D. Su, O. Borodin and C. Wang, Electrolyte Design for LiF-Rich Solid-Electrolyte Interfaces to Enable High-Performance Microsized Alloy Anodes for Batteries, *Nat. Energy*, 2020, **5**, 386–397.

43 A. M. Li, Z. Wang, T. P. Pollard, W. Zhang, S. Tan, T. Li, C. Jayawardana, S. C. Liou, J. Rao, B. L. Lucht, E. Hu, X. Q. Yang, O. Borodin and C. Wang, High Voltage Electrolytes for Lithium-Ion Batteries with Micro-Sized Silicon Anodes, *Nat. Commun.*, 2024, **15**, 1206.

44 J. Zhang, H. Zhang, L. Deng, Y. Yang, L. Tan, X. Niu, Y. Chen, L. Zeng, X. Fan and Y. Zhu, An Additive-Enabled Ether-Based Electrolyte to Realize Stable Cycling of High-Voltage Anode-Free Lithium Metal Batteries, *Energy Storage Mater.*, 2023, **54**, 450–460.

45 Z. Liu, W. Hou, H. Tian, Q. Qiu, I. Ullah, S. Qiu, W. Sun, Q. Yu, J. Yuan, L. Xia and X. Wu, An Ultralow-Concentration and Moisture-Resistant Electrolyte of Lithium Difluoro(Oxalato)Borate in Carbonate Solvents for Stable Cycling in Practical Lithium-Ion Batteries, *Angew. Chem., Int. Ed.*, 2024, **63**, e202400110.

46 A. Ghosh, B. Cohn, A. K. Prasad and L. Chuntonov, Quantifying Conformations of Ester Vibrational Probes with Hydrogen-Bond-Induced Fermi Resonances, *J. Chem. Phys.*, 2018, **149**, 184501.

47 Q. Sun, Z. Cao, Z. Ma, J. Zhang, W. Wahyudi, G. Liu, H. Cheng, T. Cai, E. Xie, L. Cavallo, Q. Li and J. Ming, Interfacial and Interphasial Chemistry of Electrolyte Components to Invoke High-Performance Antimony Anodes and Non-Flammable Lithium-Ion Batteries, *Adv. Funct. Mater.*, 2022, **33**, 2210292.

48 S. Mao, J. Zhang, J. Mao, Z. Shen, Z. Long, S. Zhang, Q. Wu, H. Cheng and Y. Lu, Anionic Aggregates Induced Interphase Chemistry Regulation toward Wide-Temperature Silicon-Based Batteries, *Adv. Energy Mater.*, 2024, **14**, 2401979.

49 L. Fan, H. Xie, Y. Hu, Z. Caixiang, A. M. Rao, J. Zhou and B. Lu, A Tailored Electrolyte for Safe and Durable Potassium Ion Batteries, *Energy Environ. Sci.*, 2023, **16**, 305–315.

50 B. Zhu, X. Wang, P. Yao, J. Li and J. Zhu, Towards High Energy Density Lithium Battery Anodes: Silicon and Lithium, *Chem. Sci.*, 2019, **10**, 7132–7148.

51 M. Ge, C. Cao, G. M. Biesold, C. D. Sewell, S. M. Hao, J. Huang, W. Zhang, Y. Lai and Z. Lin, Recent Advances in Silicon-Based Electrodes: From Fundamental Research toward Practical Applications, *Adv. Mater.*, 2021, **33**, 2004577.

52 L. Suo, W. Xue, M. Gobet, S. G. Greenbaum, C. Wang, Y. Chen, W. Yang, Y. Li and J. Li, Fluorine-Donating Electrolytes Enable Highly Reversible 5-V-Class Li Metal Batteries, *Proc. Natl. Acad. Sci. U. S. A.*, 2018, **115**, 1156–1161.

53 K. Cheng, S. Tu, B. Zhang, W. Wang, X. Wang, Y. Tan, X. Chen, C. Li, C. Li, L. Wang and Y. Sun, Material-Electrolyte Interfacial Interaction Enabling the Formation of an Inorganic-Rich Solid Electrolyte Interphase for Fast-Charging Si-Based Lithium-Ion Batteries, *Energy Environ. Sci.*, 2024, **17**, 2631–2641.

54 Z. Wang and B. Zhang, Weakly Solvating Electrolytes for Next-Generation Lithium Batteries: Design Principles and Recent Advances, *Energy Materials and Devices*, 2023, **1**, 9370003.

55 Y. Guo, M. Miao, Y. X. Wang, C. Yan, J. Liu, Y. Cao, H. Yang, X. Ai and F. S. Ke, A High-Voltage and Low-Solvating Electrolyte Towards Promising Micro-Si/Ni-Rich NMC Full Cells, *Energy Storage Mater.*, 2024, **67**, 103258.

56 C. Liu, Z. Wang, Q. Wang, J. Bai, H. Wang and X. Liu, Fluorine-Ion-Regulated Yolk-Shell Carbon-Silicon Anode Material for High Performance Lithium Ion Batteries, *J. Colloid Interface Sci.*, 2024, **668**, 666–677.